Curved Trapezoidal Magnetic Flux Concentrator Design for Current Measurement of Multi-Core Power Cable With Magnetic Sensing

Ke Zhu and Philip W. T. Pong

Department of Electrical and Electronic Engineering, The University of Hong Kong, Hong Kong

Operating current of a multi-core power cable can be monitored by sensing the magnetic fields around the cable surface. Magnetic flux concentrators (MFCs) are typically installed to collect the magnetic flux lines and amplify the magnetic field signals for magnetic sensors that are sandwiched by pairs of MFCs. However, installing a series of conventional planar MFCs around the circular cable surface would form a polygonal structure, adversely aggregating the magnetic flux lines at the corners of the polygon. In this paper, a curved MFC structure was developed to overcome the problem. First, a simple curved structure (i.e., curved strip-shaped MFCs) was derived to accommodate magnetic sensors around the cable surface. Then, it was modified into the trapezoidal shape for further improving the amplification ratio after studying the influence of MFC thickness, aspect ratio, and end-to-end ratio. The saturation effect and frequency response of MFCs were also studied. The effectiveness of the curved trapezoidal MFCs compared to the strip-shaped ones was validated experimentally, in which the average amplification ratio of the trapezoidal MFCs (5.12) was substantially larger than that of the strip-shaped MFCs (1.46). The curved trapezoidal MFCs not only eliminate the magnetic field aggregation at the polygon corners but also fit compactly the round geometry of the cable compactly. More importantly, enhancing the magnetic field signals for the magnetic sensors can potentially improve the system ability to sense the weak magnetic field variations from slight current changes. The high-order harmonics can also be potentially restored because the curved trapezoidal MFCs have a good frequency response.

Index Terms— **Current sensing, curved magnetic flux concentrator (MFC), magnetic sensor, multi-core power cable.**

I. Introduction

MULTI-CORE power cables (assembled by several electrical conductors together with an overall sheath as mechanical protection) are typically used in the distribution systems of power grids to transmit electricity [1]–[4]. Due to a lower tolerance of power suspension from industrial and residential consumers, the operating currents are monitored closely to ensure a reliable and stable power transmission [5].

Current transformers (CTs) are widely applied in power systems for the current measurement (Fig. 1). However, there are shortcomings of CTs (wound and toroidal CTs [6]) for monitoring the currents of the multi-core power cables [7]. The primary winding of a wound CT is physically connected with the current-carrying conductor [Fig. 1(a)], resulting in high insulation cost and bulky size of CTs [8], [9]. Physical contact is avoided in a toroidal CT [Fig. 1(b)] because the current-carrying conductor is through the center opening of CT; however, a toroidal CT cannot work with a multi-core power cable since the resultant magnetic field emanated from the core conductors is almost zero around the cable surface [10]. Therefore, new methods are being developed for monitoring the multi-core power distribution cables [11], [12]. A method of installing a magnetic sensor (e.g., Hall effect sensor and magnetoresistive sensors) array (since the quantity of the sensing points should be at least equal to the quantity of the conductors according to the Biot–Savart law [13]) around the cable surface [Fig. 1(c)] has been developed to monitor the phase currents inside the multi-core power cable [2], [14]. The magnetic fields around the cable surface are measured by the sensor array and then processed computationally to reconstruct the phase currents. Thanks to the compact size, low cost, and low power consumption (∼milliwatt) of thin-film magnetic sensors [12], [15], [16], the method shows a greater promise than the traditional CTs for large-scale deployment. Nevertheless, the magnetic fields around the cable surface generated by multiple electrical conductors inside the cable are inherently weak as the magnetic fields generated from balanced currents tend to mutually cancel. Moreover, the magnetic field variations would be smaller if the currents change slightly (e.g., the harmonic variation in phase currents incurred by the non-linear industrial and commercial loads such as energy conversion devices, traction drives, industrial variable speed drives, and arc welding equipment [17]). Therefore, it is necessary to further increase the magnetic field signals for magnetic sensors to facilitate the development of this technology for fully monitoring the operating currents of multi-core power cables.

Magnetic flux concentrators (MFCs) can be used to enhance the magnetic fields in the sensing region of magnetic sensors [18], [19]. The most common design is to sandwich a magnetic sensor by a pair of MFCs [20]. However, installing a series of conventional planar MFCs for a magnetic sensor array around a cable surface would form a polygonal structure, which adversely aggregates magnetic flux lines at the corners of the polygon [21]. As such, a curved MFC design was proposed in this paper for concentrating magnetic flux lines continuously without the aggregation at the corners of the polygon structure. The existing research of MFCs mainly

Manuscript received January 9, 2019; accepted January 14, 2019. Date of publication February 1, 2019; date of current version March 18, 2019. Corresponding author: P. W. T. Pong (ppong@eee.hku.hk).

Digital Object Identifier 10.1109/TMAG.2019.2893595

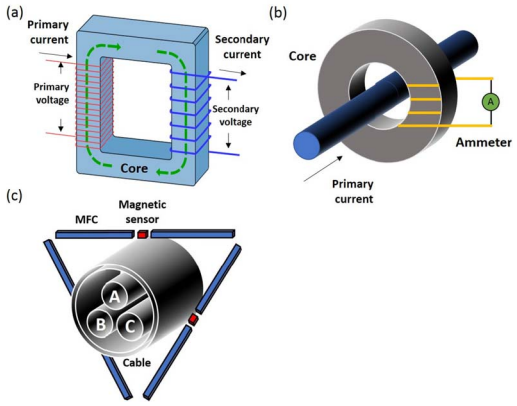

Fig. 1. Structure of CTs and MFCs. (a) Wound CT: primary winding is physically connected with the current-carrying conductor. (b) Toroidal CT: current-carrying conductor is through the core. (c) Planar bar-shaped MFCs with three magnetic sensors around the three-phase (A, B, and C), three-core power cable surface.

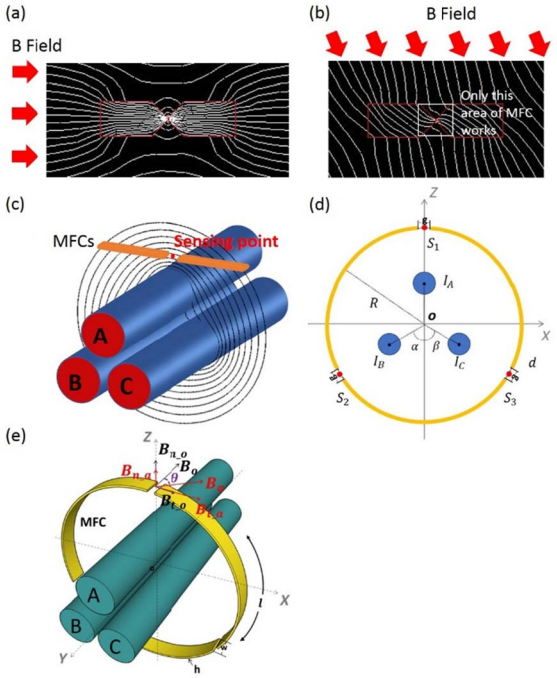

Fig. 2. Study of the curved MFCs (Mu metal [29]). (a) Magnetic fields must align with the axial direction of MFCs for achieving the largest amplification ratio. (b) MFCs operate with low efficiency when the magnetic fields are not in the axial direction of MFCs. (c) Usage of a pair of planar bar-shaped MFCs around the three-phase conductors leads to low efficiency. (d) Cross section for the layout of conductors (blue) and MFCs (yellow): radius of conductor (r), 10 mm; distance from conductor center to coordinate origin (d), 15 mm; angular displacement of conductors B and C (α and β), 60°; distance between inner radius of MFCs and coordinate origin (R), 59 mm; and gap length (g), 5.2 mm. (e) 3-D layout of conductors and MFCs: width (w), 10 mm; thickness (h), 1 mm; and amplified magnetic field (B_a) versus original magnetic field (B_o). The magnetic flux densities without (with) MFCs are decomposed into the tangential and normal components B_{t_o} and B_{n_o} (B_{t_a} and B_{n_a}).

focuses on: i) using the diamagnetism of a superconductor to generate high magnetic fields [22]; ii) improving the magnetic field detection limits by using the planar MFCs [23]; iii) studying the amplification ratio versus the linear working range [24]; and iv) the integration of MFCs on microsystems [25]. The study on the curved MFC structure is, however, very limited and merits further research. This paper is the first investigation on curved MFCs instead of planar ones. The effects of geometry, saturation, and frequency response on the amplification ratio are revealed. Moreover, the trapezoidal curved shape enables MFCs to function on a power cable with multiple core conductors which typically have a circular surface. Traditional C-shaped MFCs can only clamp around and work with a single conductor; they cannot work with multi-phase, multi-core cables because the resultant magnetic field concentrated by C-shaped MFCs would be almost zero. Our curved trapezoidal MFC design overcomes this constraint and is applicable for multi-phase, multi-core cables with a large amplification ratio.

This paper is an extension for the two-page conference digest [26]. The conference digest only provides an introduction and preliminary results of curved MFCs. It does not present the results of the effects of geometry, saturation, and frequency response on the amplification ratio. Zhu *et al.* [2] demonstrate the application of the curved trapezoidal MFCs but it does not contain any detailed study on the characterization of MFCs. This paper is the first study revealing the working principle of curved MFCs and characterizing the geometrical effect, saturation effect, and frequency response. This paper is organized as follows. First, a simple curved MFC structure (i.e., an array of curved strip-shaped MFCs) was derived based on the round geometry, and the amplification ratio is analyzed under this setup in Section II. The influence of the MFC geometry including thickness, aspect ratio, and end-to-end ratio on the amplification ratio was studied, and a modified structure (i.e., curved trapezoidal MFCs) was then proposed to increase the amplification ratio. The saturation effect of MFCs under various operating currents was also shown. Section III presents the experimental results demonstrating the effectiveness of the curved trapezoidal MFCs on a three-phase power cable. The conclusion is drawn in Section IV.

II. Curved Magnetic Flux Concentrator Design

A. Simple Design: Curved Strip-Shaped MFCs

In order to conquer the limitation that the planar MFCs would form a polygonal structure and cannot fit around the cylindrical geometry of the cable, the curved structure is designed here. The benefits of the curved MFC structure for the multi-core cable can be further explained in Fig. 2(a)–(c). When MFCs are used, their axial direction is typically paralleled with the external magnetic fields. In this way, most magnetic flux lines can congregate from their broad ends into the narrow ends, achieving the largest amplification ratio at the sensing point in the middle [Fig. 2(a)]. However, when the direction of magnetic fields is not along the axis direction of MFCs [Fig. 2(b)] as is the case for circular multi-core power cable, only a small amount of magnetic flux lines would congregate at the center of MFCs (this is because the path of magnetic fields is not easy to be altered) which leads to

a smaller amplification ratio of MFCs, resulting in MFCs working with low efficiency. The similar analysis goes for the multi-core power cables which are cylindrical in shape. If the planar MFCs are deployed for the cable where the magnetic fields are distributed circularly around the cable surface [Fig. 2(c)], MFCs would also operate in low efficiency. As such, the curved MFCs are designed in the way they are consistent with the pattern of emanated magnetic fields. Most magnetic fields would congregate at the sensing points for achieving the largest significant amplification ratio.

Since the number of sensors needs to be equal to or larger than the number of conductors when the relative positions between the sensing points and the conductors are unknown [13], three sensors at least are needed for determining the currents in a three-phase, three-core cables. Thus, three air gaps were designed for accommodating three sensors into MFCs, as shown in Fig. 2(d). This structure is equivalent to installing an array of curved strip-shaped MFCs in a circular manner [21], [27]. In order to analyze the amplification ratio of this curved strip-shaped design, magnetic fields with and without MFCs were evaluated. Traditionally, magnetic flux lines generated from a single current-carrying conductor are in the form of concentric circles (i.e., the tangential direction around the conductor). However, for the magnetic flux density generated by multiple conductors, the resultant magnetic field forms an angle with the tangential direction of the circle [28]. Therefore, the finite-element method (FEM) was used to simulate the magnetic fields with and without curved MFCs.

A typical three-phase power cable with three electrical conductors was studied as an example, as shown in Fig. 2(d) and (e). Three gaps (i.e., S_1, S_2, and S_3) were arranged symmetrically at 120° of the curved strip-shaped MFC for accommodating magnetic sensors in the middle of the gaps. The current of each phase was set to 20 A with a 120° phase difference at 50 Hz. The magnetic fields with and without MFCs were simulated by FEM. The simulation was conducted in Ansys Multiphysics, the air boundary was set on the outer surface of a cylinder with 300 mm radius, the level of smart sizing (it computes the estimated element edge lengths for all lines in the areas, and then refines for curvature and proximity of features in the geometry) was 10 with free grids, the material of phase conductor and MFCs are copper and Mu metal, respectively, the program was iterated at every 0.001 s for a cycle, and more details about spatial layouts can be found in Fig. 2(d) and (e). The result at the sensing point S_1 was analyzed. In Fig. 2(e), the magnetic field at the sensing point before and after installing MFCs are denoted by B_o and B_a, and the magnetic flux density without (with) MFCs are decomposed into the tangential and normal components B_{t_o} and B_{n_o} (B_{t_a} and B_{n_a}), respectively.

The magnetic fields with and without MFCs were simulated over a cycle of the electric current, as shown in Fig. 3. The simulation shows that the tangential component of the magnetic field was amplified by a ratio of 1.85 [B_{t_a} versus B_{t_o} as shown in Fig. 3(a)], while the normal component decreased by a ratio of 0.81 [B_{n_a} versus B_{n_o} as shown in Fig. 3(b)]. The rms resultant magnetic flux density at sensing point S_1 with (without) MFCs was 0.322 G (0.204 G),

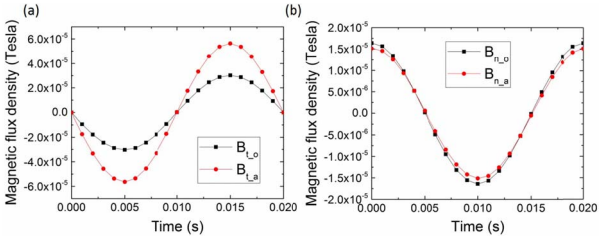

Fig. 3. Magnetic field with (without) installing curved strip-shaped MFCs simulated by FEM. (a) Tangential component of the magnetic flux density with (without) MFCs B_{to} (B_{ta}). (b) Normal component of the magnetic flux density with (without) MFCs B_{no} (B_{na}).

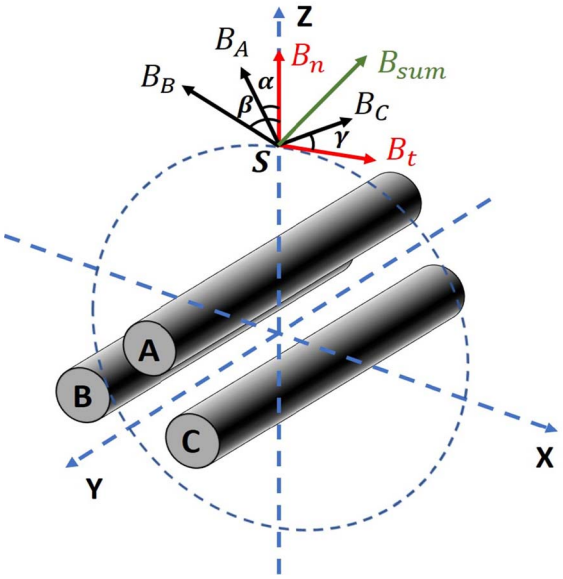

Fig. 4. Magnetic fields (B_A, B_B, and B_C) emanated from the conductors (A, B, and C) measured along the tangential (B_t) and normal (B_n) directions, respectively, at the sensing point (S).

showing that MFCs collected the magnetic flux lines and then amplified the magnetic field at the sensing point. By plotting the resultant, tangential and normal magnetic fields together [Fig. 2(e)], it was found that the resultant magnetic field vector was deflected toward the tangential direction after installing MFCs (B_a versus B_o). This shows that MFCs changed the pattern of magnetic flux lines while attracting the surrounding magnetic flux lines to amplify the magnetic field at the sensing point. The deflection was tended to MFCs because the high-permeability MFCs were of the least magnetic reluctance. It can also be observed that only the tangential component was amplified at the sensing point while the normal component was actually diminished.

Though only the tangential component of the magnetic field is amplified while the normal one decreases, it is sufficient for reconstructing the phase currents by adopting only the tangential component. This can be illustrated with a three-core power cable structure which is most commonly deployed in distribution networks nowadays [2]. The schematic for three conductors and a two-axis magnetic field measurement along the tangential and normal directions, respectively, in the Cartesian coordinate system at a sensing point is shown in Fig. 4.

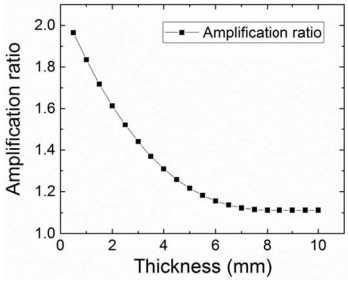

Fig. 5. Amplification ratio as a function of the MFC thickness.

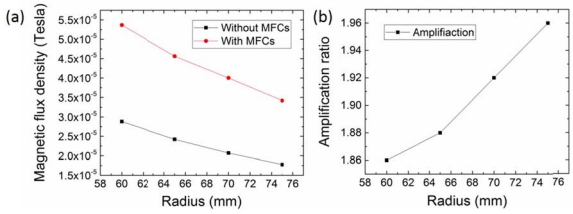

Fig. 6. Magnetic field under various radii of curved strip-shaped MFCs. (a) Maximum magnetic flux density under various radii with and without MFCs. (b) Amplification ratios under various radii.

The relative positions between conductors and sensing points are assumed known. The sensing point is located along the tangential direction of the circle with the coordinate origin as its center. The magnetic field at the sensing point generated from each conductor can be calculated by Biot–Savart law [30]. The tangential (B_t) and normal (B_n) components of the magnetic field at the sensing point can be calculated by Bio–Savart law as [30]

$$B_t = B_C\cos\gamma - B_A\sin\alpha - B_B\sin\beta \quad (1)$$

$$B_n = B_C\sin\gamma + B_A\cos\alpha + B_B\cos\beta \quad (2)$$

where $B_i(t)(i = \text{A, B, or C})$ is the magnetic field generated by the respective conductor current, and $\alpha, \beta,$ and γ are the angles formed between the direction of the magnetic field emanated from the conductor and the tangential (normal) direction of the circle at the sensing point, as depicted in Fig. 4. Since (1) and (2) are interchangeable, either the tangential (B_t) or normal component (B_n) at three sensing points should be sufficient to reconstruct the currents of three-phase conductors. Therefore, the amplification ratio A of curved MFC is defined as

$$\boldsymbol{A} = \frac{B_{t\_a}}{B_{t\_o}} \quad (3)$$

where B_{t_a} is the amplified tangential magnetic field and B_{t_o} is the original one. The amplification ratio was merely 1.85 under this setup as determined from the result shown in Fig. 3. To this effect, the MFC design needed further modification to improve the amplification ratio.

B. New Design: Curved Trapezoidal MFCs

MFCs are usually made of soft ferromagnetic materials with high relative permeability and low coercivity. Previous studies have shown that the amplification ratio can be further improved by modifying the geometrical structure of MFC [24], [26], [31], [32]. As such, the relation between the amplification ratio and the MFC's thickness, aspect ratio, and end-to-end ratio were studied as follows.

1) Thickness: The relation between the amplification ratio and the MFC thickness [h shown in Fig. 2(e)] was investigated, and the model shown in Fig. 2(e) was used again. The variation of the amplification ratio was plotted as a function of the MFC thickness (h) shown in Fig. 5. The magnetic amplification ratio decreases in an asymptotic manner as the thickness (h) increases because the magnetic flux lines are sparser when the cross-sectional area of the gap at the sensing points becomes larger. Therefore, increasing the MFC thickness does not further improve the amplification ratio.

2) Aspect Ratio: The amplification ratio is a function of the MFC aspect ratio (i.e., a ratio of the arc length [l shown in Fig. 2(e)] to the width [w shown in Fig. 2(e)] of MFC) [31]. The larger the aspect ratio, the greater is the amplification ratio. To enlarge the aspect ratio, either the width of MFC (w) can be shortened, or the length of MFC (l) can be increased. The width of MFC, however, cannot be shorter than the sensor chip; otherwise, the magnetic flux lines would not aggregate at the sensing area. MFCs can have the length extension by placing the sensors and MFCs farther away from the cable center [i.e., increasing radius R shown in Fig. 2(e)]. The farther away MFCs from the cable center (R), the longer the arc length of MFCs. The magnetic flux density with and without MFCs under various radii based on the structure shown in Fig. 2 was simulated, and the corresponding amplification ratio was calculated. Since the magnetic field from each conductor inside the cable nullifies each other, the magnetic flux density decreases with the radius [Fig. 6(a)]. The amplification ratio is enhanced with the radius which means a larger arc length and thus a larger aspect ratio [Fig. 6(b)]. However, it can be seen that the magnetic field signals for the sensors with installed MFCs indeed decreases with the radius because the magnetic field is attenuated sharply over the distance. Therefore, to further enlarge the aspect ratio by increasing the distance between the MFCs and the cable center is not effective. As such, the optimum sensing point and MFCs are recommended to be close to the cable surface for achieving the largest magnetic field signals of the magnetic sensors.

3) End-to-End Ratio: The study has shown that the amplification ratio can be further increased by enhancing the length difference of the two ends [31]. This is equivalent to modify the curved strip-shaped MFCs to curved trapezoidal designs. To investigate the relation between the amplification ratio and the ratio of the long base to short base of the trapezoidal MFC (Fig. 7), an array of curved trapezoidal MFCs was installed in the triple-conductor setup as previously shown in Fig. 2. Only the length of the long base was adjusted by fixing the length of the short base at 10 mm. The amplification ratio was attained by the FEM simulation accordingly, and the amplification ratio increased dramatically when the long base becomes larger (Fig. 8). This is because with a wider long base of a trapezoid, MFC covers a larger area and, thus, collects more magnetic flux lines from other places to converge at the short base.

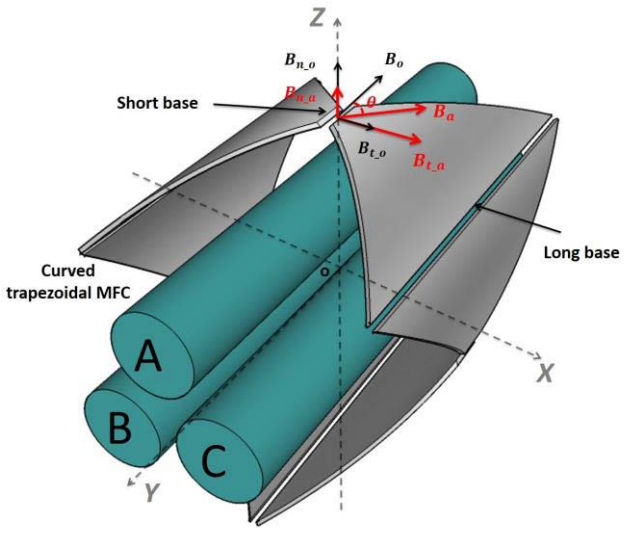

Fig. 7. Layout of three-phase conductors (phase A, B, and C) and the curved trapezoidal MFCs.

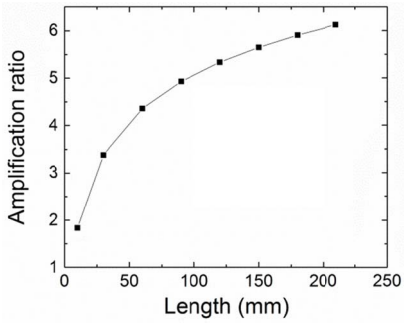

Fig. 8. Amplification ratio versus the length of the long base. (Short base is 10 mm.)

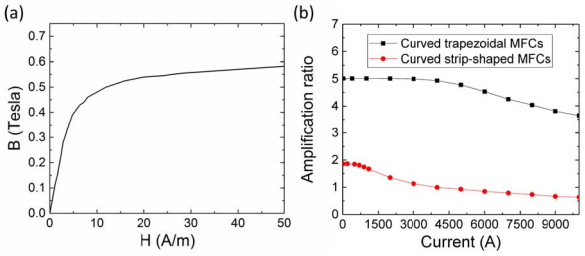

Fig. 9. Saturation effect of MFCs under various operating currents. (a) B–H curve for the Mu metal of MFCs. (b) Amplification ratio for curved strip-shaped and curved trapezoidal MFCs under various operating currents.

As such, the amplification effect became more pronounced than strip-shaped MFCs.

Although the T-shaped MFCs can achieve the same effect as the trapezoidal MFCs under almost the same specifications (i.e., material, aspect ratio, and thickness), they become saturated easily due to their relatively narrower front body where the inner magnetic flux lines are highly concentrated and congested [31]. This would result in a shorter linear range of measurement of the cable. Therefore, the use of trapezoidal MFCs was considered optimal.

C. Saturation Effect

The amplification ratio of MFCs remains constant until MFCs start to saturate under the increased external magnetic fields [31]. In our studied case, the linear working range of MFCs is the range of the operating current of the cable within which the amplification ratio keeps constant. In order to investigate the linear working range of the developed curved trapezoidal MFCs, the simulation was conducted for the MFC structure, as shown in Fig. 7 (the short base is 10 mm, and the long base is 100 mm) under various operating currents. The curved strip-shaped MFCs were also simulated as a comparison. [The structure is shown in Fig. 2(e).] MFCs are made of the Mu metal [B–H curve[29] is shown in Fig. 9(a)]. The simulation results [Fig. 9(b)] show that the linear working range of the curved trapezoidal MFCs is up to ∼3000 A, while it declines gradually as the operating current increases further. In a contrast, the working range of the curved strip-shaped MFCs is limited to around 700 A. This confirms to the study showing that the trapezoidal MFC has a larger linear range under the magnetic field than the strip-shaped MFCs[31]. The large linear range up to several thousands of amperes is critical for applying the MFCs in current monitoring of multi-core power cables since most of these power cables operate over a large range from tens to thousands of amperes [33]–[35]. Therefore, though the curved trapezoidal MFCs consume more fabrication materials than the curved strip-shaped ones, it is worthwhile because the curved trapezoidal MFCs achieve both larger amplification ratio and linear range.

D. Frequency Response

The harmonic current is a multiple of the fundamental frequency as a result of the non-linear electric loads [1]. These high-frequency harmonic currents (e.g., 150, 250, 350, 450, … Hz for a fundamental frequency of 50 Hz) result in the corresponding variation of magnetic fields around the cable surface. In order to evaluate the MFC performance under different frequencies, the simulation was conducted for the curved trapezoidal (setting is shown in Fig. 7) and strip-shaped [setting is shown in Fig. 2(e)] MFCs, respectively, from 50 Hz to 40 kHz. The variation of permeability with frequency was not considered because the frequency range we investigated was far below 100 kHz [36], [37]. The result shown in Fig. 10(a) shows that the curve trapezoidal MFC outperformed the strip-shaped one because its amplification ratio remains stable up to almost 10 kHz (equivalent to the 200th harmonics for a fundamental frequency of 50 Hz) while the amplification ratio of the curved strip-shaped one starts to decade from ∼1 kHz. The amplification ratio alters because a secondary magnetic field generated by the eddy current in MFC counteracts the field generated by the current-carrying cables at high frequency, and the eddy current becomes stronger with higher frequency [38]–[40]. The amplification ratio of the curved trapezoidal MFC remains stable at frequencies from 50 Hz to 20 kHz compared to that of the strip-based MFC. The eddy current in the curved trapezoidal MFC mainly occurs at the long base of MFC [Fig. 10(b)]

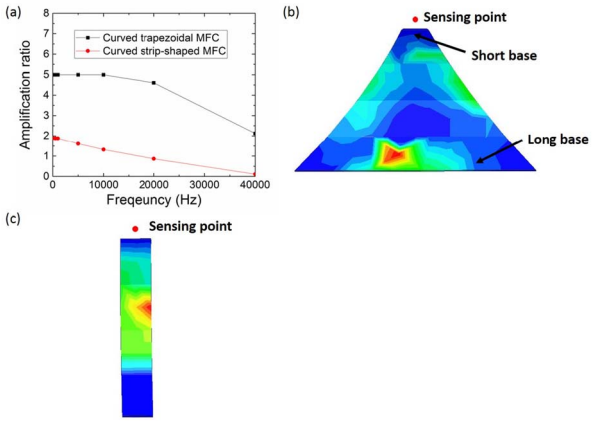

Fig. 10. Frequency bandwidth study for the curved trapezoidal and strip-shaped MFCs. (a) Amplification ratio under different frequencies. (b) Eddy current density on the curved trapezoidal MFC by the FEM simulation (20 A phase current and 1000 Hz frequency at 0.0004 s). (c) Eddy current density on the curved strip-shaped MFC by the FEM simulation (20 A phase current and 1000 Hz frequency at 0.0004 s).

because the flow of electrons tends to take place at less constrained region [41], [42] and the trapezoidal MFC has a larger surface area at the long base side. Thus, the eddy current is far away from the sensing point which is located very close to the short base. On the contrary, the eddy current mainly occurs at the middle of the strip-shaped MFC [Fig. 10(c)], and it is much closer to the sensing point. As such, the curved trapezoidal MFC exhibits a larger frequency bandwidth than the strip-shaped MFC in the current measurement of a three-phase cable through the magnetic sensing.

III. Experimental Verification and Discussion

The experiment was conducted on a three-phase, three-core, current-energized power cable (BS6622 three-core armored 22 kV XLPE stranded aluminum conductor [43]) to verify the effectiveness of the curved trapezoidal MFCs. The schematic of the power cable is shown in Fig. 11(a), where the three-phase conductors were insulated by the polypropylene and then protected by a metallic armor. The three-phase power cable was operated at 8.5 A with a 120° phase difference at 50 Hz. The curved trapezoidal and strip-shaped MFCs were fabricated, respectively, to test their performance, and the three-axis magnetic sensor (HMC2003 Honeywell) was used [44]. The sensor outputs in the xz plane were recorded, while the y-axis output was not because there was no component of the magnetic field emanated from the conductors along the y-axis (cable direction). The configuration of the Mu-metal [45] curved trapezoidal MFCs is shown in Fig. 11(b) and (c). The length of MFC's short base was 10 mm, which was equal to the width of the x-axis and y-axis sensor for measurement. As discussed in Section II, it is sufficient to clamp only one axis (x-axis in this case) of the sensor because only the tangential component of the magnetic field would be adopted to reconstruct the phase current. The length of the long base (100 mm) of the trapezoidal MFC was 10 times that of the short base (10 mm). The thickness was designed with 1 mm in order to achieve a large amplification

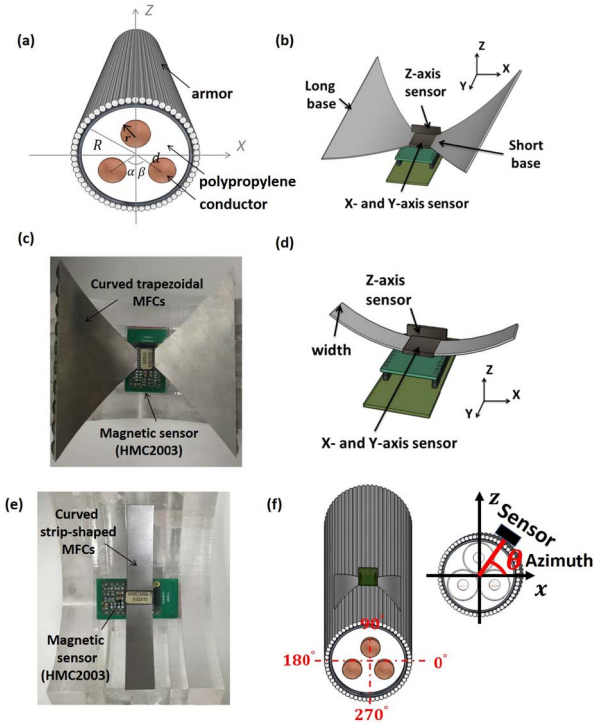

Fig. 11. Experiment on the amplification ratio with the curved trapezoidal and the curved strip-shaped MFCs. (a) Three-phase, three-core power cable configuration: radius of conductor (r), 10 mm; distance of conductor center to the coordinate origin (d), 15 mm; angular displacement for conductors 2 and 3 (α and β), 60°; and distance between MFCs and the coordinate origin (R), 40 mm. (b) Schematic of the three-axis magnetic sensor (HMC2003) and the curved trapezoidal MFCs (long base: 100 mm, short base: 10 mm, and thickness: 1mm). (c) Photograph of the three-axis magnetic sensor (HMC2003) and the curved trapezoidal MFCs. (d) Schematic of the three-axis magnetic sensor (HMC2003) and the curved strip-shaped MFCs (width: 10 mm and thickness: 1 mm). (e) Photograph of the three-axis magnetic sensor (HMC2003) and the curved strip-shaped MFCs. (f) Magnetic field measured around the cable surface was measured as a function of the azimuth with and without MFCs, respectively. (The sensor was 60 mm away from the cable center.)

as discussed in Section II-B.1 and as indicated in Fig. 5. The configuration of the Mu-metal curved strip-shaped MFCs for comparison is shown in Fig. 11(d) and (e). The width of the curved strip-shaped MFCs was the same as the short base of the curved trapezoidal MFCs, i.e., 10 mm. The other configuration such as the arc length and the thickness was the same as those of the curved trapezoidal MFCs. In order to compare the amplification of the curved trapezoidal and strip-shaped MFCs, the rms magnetic flux density around the cable surface in a full circle as a function of the azimuth [the angle between the sensor position and the horizontal axis, θ shown in Fig. 11(f)] was measured with and without MFCs.

The magnetic field measured around the cable surface with and without MFCs by the x-axis of the sensors (y-axis is along the cable direction) is shown in Fig. 12(a). The magnetic field with the curved trapezoidal MFCs was amplified to a larger extent than that with the curved strip-shaped MFCs. The amplification ratio was further separately calculated at each azimuth for the strip-shaped and trapezoidal MFCs, and the discussion about the result shown in Fig. 10(b) is as follows.

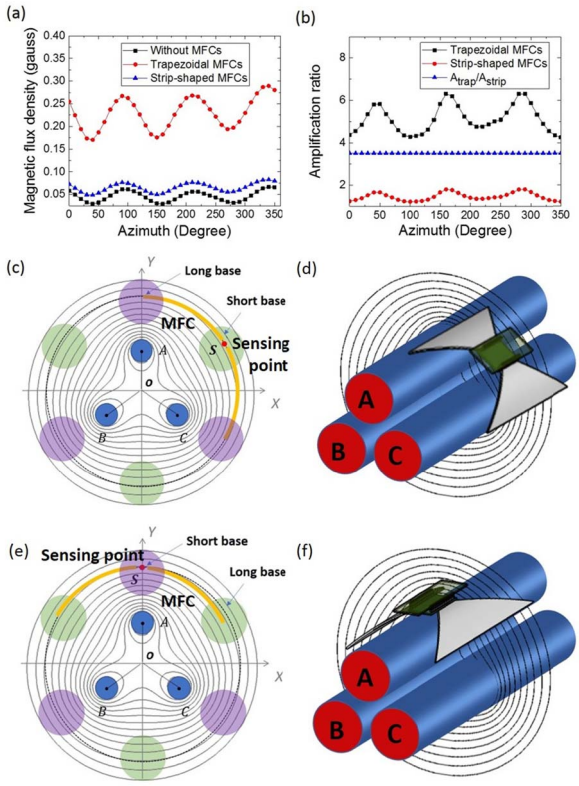

Fig. 12. Experimental study on the amplification ratio of curved trapezoidal and strip-shaped MFCs operating with the three individual conductors in a three-phase, three-core power cable. (a) Tangential component of the magnetic field amplified by the curved strip-shaped and trapezoidal MFCs, respectively. (b) Amplification ratio by trapezoidal and strip-shaped MFCs and their comparison ratio ($A_{\text{trap}}/A_{\text{strip}}$). (c) Larger amplification ratio is obtained when the long base of the curved trapezoidal MFC covers the region with dense magnetic flux lines (nearby the conductor as indicated in purple). (d) 3-D drawing showing the long base of the curved trapezoidal MFC covers the region with dense magnetic flux lines. (e) Smaller amplification ratio is obtained when the long base of the curved trapezoidal MFC covers the region with less dense magnetic flux lines (between conductors as indicated in green). (f) 3-D drawing showing the long base of the curved trapezoidal MFC covers the region with less dense magnetic flux lines (between conductors).

1) *Amplification Ratio at an Azimuth:* As can be observed in Fig. 12(a), the average amplification ratio of the trapezoidal MFCs that of 5.12 was substantially larger than that of the strip-shaped MFCs that of 1.46. (The small discrepancies of amplification ratios between experiment and simulation were because the actual sensing point inside the sensor in the experiment may be slightly different from simulation.) At a fixed azimuth, the ratio ($A_{\text{trap}}/A_{\text{strip}}$) of the amplification induced by the trapezoidal MFCs to the strip-shaped MFCs was calculated to be a constant value, i.e., 3.5. The experimental result verified that the trapezoidal MFCs can provide a larger amplification than the strip-shaped ones.
2) *Amplification Ratio Over Azimuths:* As can be observed in Fig. 12(b), the amplification ratio changed over the azimuths, and it exhibited a pattern composing of three peaks and troughs. The largest amplification ratio induced by the curved strip-shaped and trapezoidal MFCs both occurred at the azimuths of 50°, 160°, and 290°. The amplification ratios of the curved strip-shaped MFCs at these three azimuths were smaller (1.66, 1.80, and 1.80, respectively), and those of the curved trapezoidal MFCs were larger (5.82, 6.31, and 6.30, respectively). The pattern of three peaks and troughs of the amplification ratio can be understood by looking at the magnetic field distribution pattern of the three-phase conductors that were simulated shown in Fig. 12(c)–(f). The denser magnetic flux density areas (purple circles) are directly opposite to the conductors while their neighboring areas are less dense (green circles). MFCs operate by collecting the magnetic flux lines from the region they cover and then concentrate them at the sensing point. A larger amplification ratio can be obtained by placing the long base at the dense magnetic flux density area [Fig. 12(c) and (d)] while the weaker amplification ratio can be obtained by placing the long base at the area with less dense magnetic flux lines [Fig. 12(e) and (f)]. Since the magnetic flux density on the cable surface repeats at an interval of $2/3\pi$ for a three-phase, three-core conductors, the amplification ratio also shows a similar pattern with three peaks and troughs. Therefore, in order to achieve a larger amplification ratio in practice, it is suggested to place the trapezoidal MFCs' long base at the denser magnetic flux line areas that are right opposite to the conductors.

In terms of applying this technique in practice, there are some points to be addressed.

1) *Pre-Calibration:* in order to restore the original magnetic fields for reconstructing the phase currents, it is necessary to obtain the amplification ratio at each sensing point. Due to the potential non-ideality of cables or MFCs (e.g., the cable conductors may not be definitely symmetrical at 120°, or the MFCs may not be fabricated with the exact radius of curvature as the power cable), the amplification ratio cannot be simply attained by simulation. As such, a pre-calibration (to measure the tangential magnetic fields of each sensor with and without MFCs) is required for determining the amplification ratio at each sensing point.
2) *Conductor Location:* In order to restore the three-phase currents from the measured magnetic fields, it is necessary to attain the conductor positions for (1) and (2). This can be achieved by measuring magnetic fields around the cable surface with a magnetic sensor array and then calculated with non-linear equations [13] or a stochastic optimization algorithm [2] beforehand. Afterward, the minimum number of magnetic sensors needed is the same as the number of phase conductors in the cable (e.g., three sensors for a three-phase, three-core power cable). Each curved trapezoidal MFC can have longer arc length and thus congregate more magnetic flux when there are fewer sensors around the cable surface.
3) *Electromagnetic Background:* There might be other current-carrying power cables or power sources nearby which can generate the magnetic field noises interfering the measurement. Nevertheless, this problem can be

overcome by using a magnetic shielding. As demonstrated in our previous work in [2] as well as works by other groups in [46]–[48], magnetic shielding made with soft materials can effectively shield against electromagnetic background noises and protect the magnetic measurement.

4) *Radius of MFCs:* As discussed in Section II-B, the radius of curvature of the curved trapezoidal MFCs should be close to the power cable for achieving the largest amplified magnetic field. The fabricated curved trapezoidal MFCs with the radius of curvature smaller or larger than that of the cable can still be installed. There would just be some redundant space between the cable and MFCs if the radius of MFCs is larger than that of the cable; however, if the radius of MFCs is smaller than that of the cable, the arc length of MFCs cannot cover the full perimeter of the cable. Under this situation, the arc length is recommended to further increase for a larger aspect ratio as discussed in Section II-B in order to achieve the optimal amplification ratio. As such, it is recommended to re-fabricate MFCs if their radii are smaller than the power cables.

IV. Conclusion

This paper has presented a curved MFC design in order to amplify the magnetic field signals at the sensing point of magnetic sensors for improving the current monitoring in a multi-core power cable. First, a simple structure (i.e., the curved strip-shaped MFCs) was derived based on the round geometry, and the amplification ratio of the curved MFCs was defined. Then, the curved trapezoidal MFCs were proposed by modifying the curved strip-shaped MFCs after analyzing the influence of MFC thickness, aspect ratio, and end-to-end ratio of the curved strip-shaped MFCs. The curved trapezoidal MFCs also show both a larger working range of operating current and frequency response than the strip-shaped ones. Stronger amplification ratio of average 5.12 of the curved trapezoidal MFCs was verified in the experiment compared to average 1.3 with the strip-shaped MFC.

The curved MFC structure can also clamp the multi-core power cable compactly with minimal waste space between the cable and the MFCs. The enhanced magnetic field signals of magnetic sensors can potentially improve the system ability to sense the slight current changes from weak magnetic field variations. For example, high-order harmonics can also be potentially measured because the curved trapezoidal MFCs have a good frequency response.

Acknowledgment

This work was supported in part by The University of Hong Kong through the Seed Funding Program for Basic Research, the Seed Funding Program for Applied Research, and the Small Project Funding Program, in part by ITF Tier 3 Funding under Grant ITS-203-14, Grant ITS-104/13, and Grant ITS-214/14, in part by the RGC General Research Fund under Grant 17204617 and Grant 17210014, and in part by the University Grants Committee of Hong Kong under Grant AoE/P-04/08.

References

[1] W. A. Thue, *Electrical Power Cable Engineering*. Boca Raton, FL, USA: CRC Press, 2011.

[2] K. Zhu, H. Wei, W. K. Lee, and P. W. T. Pong, "On-site non-invasive current monitoring of multi-core underground power cables with a magnetic-field sensing platform at a substation," *IEEE Sensors J.*, vol. 17, no. 6, pp. 1837–1848, Mar. 2017.

[3] S. B. Dalal, R. S. Gorur, and M. L. Dyer, "Aging of distribution cables in service and its simulation in the laboratory," *IEEE Trans. Dielectrics Electr. Insul.*, vol. 12, no. 1, pp. 139–146, Feb. 2005.

[4] Z. Achillides, E. Kyriakides, and G. E. Georghiou, "Partial discharge modeling: An improved capacitive model and associated transients along medium voltage distribution cables," *IEEE Trans. Dielectrics Electr. Insul.*, vol. 20, no. 3, pp. 770–781, Jun. 2013.

[5] S. M. Amin and B. F. Wollenberg, "Toward a smart grid: Power delivery for the 21st century," *IEEE Power Energy Mag.*, vol. 3, no. 5, pp. 34–41, Sep./Oct. 2005.

[6] Electronics. (2018). *The Current Transformer*. Accessed: Aug. 9, 2017. [Online]. Available: https://www.electronics-tutorials.ws/transformer/current-transformer.html

[7] P. C. Y. Ling and A. Basak, "Investigation of magnetizing inrush current in a single-phase transformer," *IEEE Trans. Magn.*, vol. MAG-24, no. 6, pp. 3217–3222, Nov. 1988.

[8] A. A. Adly, "Computation of inrush current forces on transformer windings," *IEEE Trans. Magn.*, vol. 37, no. 4, pp. 2855–2857, Jul. 2001.

[9] Y. Yao, C. S. Koh, G. Ni, and D. Xie, "3-D nonlinear transient eddy current calculation of online power transformer under DC bias," *IEEE Trans. Magn.*, vol. 41, no. 5, pp. 1840–1843, May 2005.

[10] WIKIPEDIA. (2017). *Current Clamp*. Accessed: Feb. 15, 2017. [Online]. Available: https://en.wikipedia.org/wiki/Current_clamp

[11] C. Reig, M.-D. Cubells-Beltrán, and D. R. Muñoz, "Magnetic field sensors based on giant magnetoresistance (GMR) technology: Applications in electrical current sensing," *Sensors*, vol. 9, no. 10, pp. 7919–7942, Oct. 2009.

[12] J. Lenz and A. S. Edelstein, "Magnetic sensors and their applications," *IEEE Sensors J.*, vol. 6, no. 3, pp. 631–649, Jun. 2006.

[13] L. Meng, P. Gao, M. M. Haji, and W. Xu, "Magnetic sensor array-based AC current measurement for multiconductor cables using evolutionary computation method," *IEEE Trans. Instrum. Meas.*, vol. 64, no. 10, pp. 2747–2758, 2015.

[14] X. Sun *et al.*, "Operation-state monitoring and energization-status identification for underground power cables by magnetic field sensing," *IEEE Sensors J.*, vol. 13, no. 11, pp. 4527–4533, Nov. 2013.

[15] J. E. Lenz, "A review of magnetic sensors," *Proc. IEEE*, vol. 78, no. 6, pp. 973–989, Jun. 1990.

[16] P. Ripka and M. Janosek, "Advances in magnetic field sensors," *IEEE Sensors J.*, vol. 10, no. 6, pp. 1108–1116, Jun. 2010.

[17] A. K. Hiranandani, "Effects of harmonics on the current carrying capacity of insulated power cables used in three phase electrical power distribution systems," in *Proc. 18th Int. Conf. Exhib. Electr. Distrib. (CIRED)*, Jun. 2005, pp. 1–5.

[18] R. S. Popovic, Z. Randjelovic, and D. Manic, "Integrated Hall-effect magnetic sensors," *Sens. Actuators A, Phys.*, vol. 91, nos. 1–2, pp. 46–50, Jun. 2001.

[19] R. S. Popovic, P. M. Drljaca, and C. Schott, "Bridging the gap between AMR, GMR, and Hall magnetic sensors," in *Proc. 23rd Int. Conf. Microelectron.*, May 2002, pp. 55–58.

[20] P. Ripka and K. Závěta, "Chapter three magnetic sensors: Principles and applications," *Handbook of Magnetic Materials*, vol. 18. Amsterdam, The Netherlands: North Holland, 2009, pp. 347–420.

[21] Allegro. (2016). *Guidelines for Designing a Concentrator for High-Current Sensing Applications with an Allegro Hall-Effect Sensor IC*. Accessed: Jan. 15, 2017. [Online]. Available: http://www.allegromicro.com/en/Design-Center/Technical-Documents/Hall-Effect-Sensor-IC-Publications/Current-Sensor-Concentrator.aspx

[22] T. Kiyoshi, S. Choi, S. Matsumoto, T. Asano, and D. Uglietti, "Magnetic flux concentrator using Gd-Ba-Cu-O bulk superconductors," *IEEE Trans. Appl. Supercond.*, vol. 19, no. 3, pp. 2174–2177, Jun. 2009.

[23] A. Guedes, J. M. Almeida, S. Cardoso, R. Ferreira, and P. P. Freitas, "Improving magnetic field detection limits of spin valve sensors using magnetic flux guide concentrators," *IEEE Trans. Magn.*, vol. 43, no. 6, pp. 2376–2378, Jun. 2007.

[24] P. M. Drljača, F. Vincent, P.-A. Besse, and R. S. Popović, "Design of planar magnetic concentrators for high sensitivity Hall devices," *Sens. Actuators A, Phys.*, vols. 97–98, pp. 10–14, Apr. 2002.

[25] R. S. Popovic, P. M. Drljaca, C. Schott, and R. Racz, "Integrated HALL sensor/flux concentrator microsystems," *Inform. Midem. J.*, vol. 31, no. 4, pp. 215–219, 2001.
[26] K. Zhu and P. W. T. Pong, "Curved trapezoidal magnetic flux concentrator design for improving sensitivity of magnetic sensor in multi-conductor current measurement," in *Proc. 5th Int. Symp. Next-Gener. Electron.*, May 2016, pp. 1–2.
[27] Permanent Magnets Ltd. (2017). *Laminated Flux Concentrators*. Accessed: Aug. 9, 2017. [Online]. Available: https://www.pmlindia.com/products/laminated-flux-concentrators
[28] K. Zhu, W. K. Lee, and P. W. T. Pong, "Energization-status identification of three-phase three-core shielded distribution power cables based on non-destructive magnetic field sensing," *IEEE Sensors J.*, vol. 17, no. 22, pp. 7405–7417, Nov. 2017.
[29] Ansys. (2017). *Introduction of Maxwell*. Accessed: Oct. 6, 2017. [Online]. Available: http://www.ansys.com/products/electronics/ansys-maxwell
[30] T. Charitat and F. Graner, "About the magnetic field of a finite wire," *Eur. J. Phys.*, vol. 24, p. 267, Jul. 2003.
[31] X. Sun, L. Jiang, and P. W. T. Pong, "Magnetic flux concentration at micrometer scale," *Microelectron. Eng.*, vol. 111, pp. 77–81, Nov. 2013.
[32] Z. Y. Zhang, S. Matsumoto, S. Choi, R. Teranishi, and T. Kiyoshi, "A new structure for a magnetic field concentrator using NbTi sheet superconductors," *Phys. C, Supercond. Appl.*, vol. 471, nos. 21–22, pp. 1547–1549, 2011.
[33] S. Mukoyama *et al.*, "Model cable tests for a 275 kV 3 kA HTS power cable," *IEEE Trans. Appl. Supercond.*, vol. 21, no. 3, pp. 976–979, Jun. 2011.
[34] J. F. Maguire *et al.*, "Development and demonstration of a HTS power cable to operate in the long island power authority transmission grid," *IEEE Trans. Appl. Supercond.*, vol. 17, no. 2, pp. 2034–2037, Jun. 2007.
[35] J. P. Stovall *et al.*, "Installation and operation of the Southwire 30-meter high-temperature superconducting power cable," *IEEE Trans. Appl. Supercond.*, vol. 11, no. 1, pp. 2467–2472, Mar. 2001.
[36] Yuxiang. (2018). *Iron Powder Cores*. Accessed: Feb. 6, 2018. [Online]. Available: http://www.magnet-tech.com/core/Metallic/characteristics2.htm
[37] MH&W International Corp. (2011). *Permeability vs. Frequency Curves*. Accessed: Feb. 20, 2018. [Online]. Available: http://www.mhw-intl.com/assets/CSC/CSC%20Perm%20vrs%20Frequency%202011.pdf
[38] WIKIPEDIA. (2018). *Eddy Current*. Accessed: Jan. 24, 2018. [Online]. Available: https://en.wikipedia.org/wiki/Eddy_current
[39] D. C. Jiles, "Modelling the effects of eddy current losses on frequency dependent hysteresis in electrically conducting media," *IEEE Trans. Magn.*, vol. 30, no. 6, pp. 4326–4328, Nov. 1994.
[40] D. Ishak, Z. Q. Zhu, and D. Howe, "Eddy-current loss in the rotor magnets of permanent-magnet brushless machines having a fractional number of slots per pole," *IEEE Trans. Magn.*, vol. 41, no. 9, pp. 2462–2469, Sep. 2005.
[41] *Why Are Eddy Currents Circular?*, Quora, Mountain View, CA, USA, 2018.
[42] K. Boughrara, N. Takorabet, R. Ibtiouen, O. Touhami, and F. Dubas, "Analytical analysis of cage rotor induction motors in healthy, defective, and broken bars conditions," *IEEE Trans. Magn.*, vol. 51, no. 2, pp. 1–17, Feb. 2015.
[43] PRYSMIAN. (2017). *BS6622 Three Core Armoured 22 kV XLPE Stranded Aluminium Conductor*. Accessed: Aug. 9, 2017. [Online]. Available: http://uk.prysmiangroup.com/en/business_markets/markets/ti/datasheets/3_core_arm_22kv_ccBS662BS7835.pdf
[44] Honeywell. (2016). *Three-Axis Magnetic Sensor Hybrid*. Accessed: Mar. 28, 2017. [Online]. Available: http://www.cs.unc.edu/~vicci/comp261/compass/hmc2003.pdf
[45] Magnetic Shields. (2015). *Mu Metal*. Accessed: Aug. 9, 2017. [Online]. Available: http://mumetalsheet.co.uk/
[46] V. Kelha, J. Pukki, R. Peltonen, A. Penttinen, R. Ilmoniemi, and J. Heino, "Design, construction, and performance of a large-volume magnetic shield," *IEEE Trans. Magn.*, vol. MAG-18, no. 1, pp. 260–270, Jan. 1982.
[47] O. Bottauscio, M. Chiampi, and A. Manzin, "Numerical analysis of magnetic shielding efficiency of multilayered screens," *IEEE Trans. Magn.*, vol. 40, no. 2, pp. 726–729, Mar. 2004.
[48] R. Boll and H. Warlimont, "Applications of amorphous magnetic materials in electronics," *IEEE Trans. Magn.*, vol. 17, no. 6, pp. 3053–3058, Nov. 1981.

Ke Zhu (M'12) was born in Yichang, China, in 1990. He received the B.Eng. degree in electrical engineering from China Three Gorges University, Yichang, China, in 2013, and the Ph.D. degree in electrical and electronic engineering from The University of Hong Kong, Hong Kong, in 2018.

He is currently a Post-Doctoral Researcher with The University of Hong Kong. His current research interests include computational electromagnetics, electric power transmission monitoring, and application of magnetoresistive sensors in a smart grid.

Philip W. T. Pong (SM'13) received the B.Eng. degree (Hons.) in electrical and electronic engineering from The University of Hong Kong (HKU), Hong Kong, in 2002, and the Ph.D. degree in engineering from the University of Cambridge, Cambridge, U.K., in 2005.

He was a Post-Doctoral Researcher with the Magnetic Materials Group, National Institute of Standards and Technology, Gaithersburg, MD, USA, for three years. In 2008, he joined the Department of Electrical and Electronic Engineering, HKU, where he is currently an Associate Professor, focusing on the development of magnetoresistive (MR) sensors and the applications of MR sensors in smart grid and smart living.

Dr. Pong is a Chartered Physicist, a Chartered Energy Engineer, a Registered Professional Engineer, a fellow of the Institute of Materials, Minerals and Mining, a fellow of the NANOSMAT Society, and a Corporate Member of Hong Kong Institution of Engineers (HKIE) in the Electrical Division, the Electronics Division, and the Energy Division. He serves as an Editorial Board Member for three SCI journals. He was a recipient of the HKIE Young Engineer of the Year Award in 2016. He is serving on the Administrative Committee of the IEEE Magnetics Society.